01 Jun 2008

Fault Growth and Propagation During Incipient Continental Rifting: Insights from a Combined Aeromagnetic and Shuttle Radar Topography Mission Digital Elevation Model Investigation of the Okavango Rift Zone, Northwest Botswana

Baraka D. Kinabo

John Patrick Hogan
Missouri University of Science and Technology, jhogan@mst.edu

Eliot A. Atekwana
Missouri University of Science and Technology

Mohamed G. Abdel Salam
Missouri University of Science and Technology, abdelsam@mst.edu

et. al. For a complete list of authors, see https://scholarsmine.mst.edu/geosci_geo_peteng_facwork/90

Recommended Citation

B. D. Kinabo et al., "Fault Growth and Propagation During Incipient Continental Rifting: Insights from a Combined Aeromagnetic and Shuttle Radar Topography Mission Digital Elevation Model Investigation of the Okavango Rift Zone, Northwest Botswana," *Tectonics*, vol. 27, no. 3, American Geophysical Union (AGU), Jun 2008.
The definitive version is available at https://doi.org/10.1029/2007TC002154

Fault growth and propagation during incipient continental rifting: Insights from a combined aeromagnetic and Shuttle Radar Topography Mission digital elevation model investigation of the Okavango Rift Zone, northwest Botswana

B. D. Kinabo,[1,2] J. P. Hogan,[1] E. A. Atekwana,[3] M. G. Abdelsalam,[1] and M. P. Modisi[4]

Received 29 May 2007; revised 20 November 2007; accepted 17 January 2008; published 28 June 2008.

[1] Digital Elevation Models (DEM) extracted from the Shuttle Radar Topography Mission (SRTM) data and high-resolution aeromagnetic data are used to characterize the growth and propagation of faults associated with the early stages of continental extension in the Okavango Rift Zone (ORZ), northwest Botswana. Significant differences in the height of fault scarps and the throws across the faults in the basement indicate extended fault histories accompanied by sediment accumulation within the rift graben. Faults in the center of the rift either lack topographic expressions or are interpreted to have become inactive, or have large throws and small scarp heights indicating waning activity. Faults on the outer margins of the rift exhibit either (1) large throws or significant scarp heights and are considered older and active or (2) throws and scarp heights that are in closer agreement and are considered young and active. Fault linkages between major fault systems through a process of ''fault piracy'' have combined to establish an immature border fault for the ORZ. Thus, in addition to growing in length (by along-axis linkage of segments), the rift is also growing in width (by transferring motion to younger faults along the outer margins while abandoning older faults in the middle). Finally, utilization of preexisting zones of weakness allowed the development of very long faults (>100 km) at a very early stage of continental rifting, explaining the apparent paradox between the fault length versus throw for this young rift. This study clearly demonstrates that the integration of the SRTM DEM and aeromagnetic data provides a 3-D view of the faults and fault systems, providing new insight into fault growth and propagation during the nascent stages of continental rifting. **Citation:** Kinabo, B. D., J. P. Hogan, E. A. Atekwana, M. G. Abdelsalam, and M. P. Modisi (2008), Fault growth and propagation during incipient continental rifting: Insights from a combined aeromagnetic and Shuttle Radar Topography Mission digital elevation model investigation of the Okavango Rift Zone, northwest Botswana, *Tectonics*, *27*, TC3013, doi:10.1029/2007TC002154.

1. Introduction

[2] Understanding the factors that control the growth and propagation of normal faults at the earliest stages of continental rifting will lead to a better overall understanding of the processes that control the development of continental rifts, an essential component of the plate tectonics paradigm. This is because the location, orientation, and evolution of normal faults that form during continental rifting exert a strong influence on the development of regional features of the rift including: (1) geomorphology, (2) drainage patterns, (3) basin location, (4) stratigraphy, (5) location of magmatism, and if the process of continental rifting is successful, (6) the geometry of the passive margin. Additionally, because rift basins and rifted continental margins are considered to be the most prolific areas of hydrocarbon accumulation [*Trudgill and Underhill*, 2002] this knowledge can lead to increased efficiency in petroleum exploration and the development of proven reserves.

[3] Our understanding of the earliest stages of fault initiation and development and the details of fault linkage and propagation during continental rifting within the cratonic lithosphere lags behind our knowledge of many other processes associated with continental rifting for two main reasons. The first is that we can only study the present-day geometry of the faults [*Schlische and Anders*, 1996]. The second is that investigation of continental rifting has typically focused on a few well documented continental rifts (e.g., the East African Rift System (EARS), Baikal Rift, Rio Grande Rift and North Sea/Viking Graben) where border faults are either fully developed or in an advanced stage of development. Thus, observations critical to constraining processes important to the early stages of fault development during continental rifting are commonly made obscure in these more mature rifts by accumulation of thick sedimentary sequences, volcanic sequences, or by multiple rifting events.

[4] Much of our knowledge on incipient continental rifting comes from Mesozoic-Palaeogene hydrocarbon producing

[1]Department of Geological Sciences and Engineering, Missouri University of Science and Technology, Rolla, Missouri, USA.
[2]Now at Technical Geophysics Group, Deepwater Gulf of Mexico, Chevron North America Exploration and Production, Houston, Texas, USA.
[3]Boone Pickens School of Geology, Oklahoma State University, Stillwater, Oklahoma, USA.
[4]Department of Geology, University of Botswana, Gaborone, Botswana.

0278-7407/08/2007TC002154

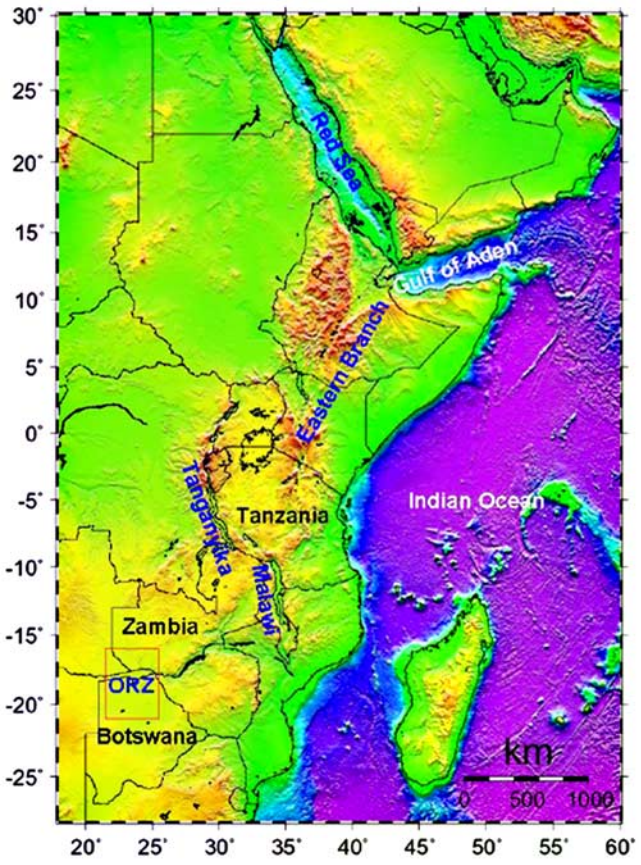

Figure 1. SRTM DEM map of the East Africa Rift System showing the location of the study area (red rectangle).

basins such as North Sea. Information on incipient continental rift zones is limited to a few studies such as those of *Foster et al.* [1997], *Ebinger et al.* [1997], *Modisi et al.* [2000], and *Kinabo et al.* [2007]. This is partly because there are only a few examples of young continental rifts which are suitable for the investigation of the process of border fault development and evolution. The Okavango Rift Zone (ORZ), in northwest Botswana (Figures 1 and 2) is such a zone of incipient continental rifting [*Scholz et al.*, 1976; *Modisi et al.*, 2000]. Recent studies suggest that faults associated with this rift are still in a juvenile stage [*Kinabo et al.*, 2007]. Thus, the ORZ can serve as a modern day analog for the earliest stages of more evolved continental rift basins and provides us with a unique opportunity to investigate the earliest developmental stages of continental rifts.

[5] Studies on fault growth and evolution have traditionally relied on field studies such as structural mapping and stratigraphic analysis [e.g., *Anders and Schlische*, 1994; *Cartwright et al.*, 1995; *Dawers and Anders*, 1995; *Peacock and Sanderson*, 1991; *Gawthorpe et al.*, 1997; *Jackson et al.*, 2002], analog models using sand and clay, and numerical models to understand formation, early interactions of segments, and growth of the faults [*Cowie and Scholz*, 1992; *Cowie*, 1998a, 1998b; *Trudgill and Cartwright*, 1994; *Cartwright et al.*, 1995; *Morley*, 1999; *Mulugeta and Woldai*, 2001; *Moustafa*, 2002; *Withjack et al.*, 1995]. Scientists have also used an integration of seismic data analysis and field work [e.g., *Ebinger et al.*, 1984; *Davies et al.*, 2000; *Morley*, 2002] or a combination of analog/numerical models with fieldwork for understanding fault growth and propagation and their effect on the stratigraphic architecture and dispersal patterns [e.g., *McClay et al.*, 2002]. However, in areas where the faults are mostly buried beneath large accumulations of sediment, have subdued surface relief, or where rock outcrops are limited, such as in the case of ORZ [*Kinabo et al.*, 2007; *Modisi et al.*, 2000], it is often difficult to accomplish structural mapping, stratigraphic analysis, and seismic studies through land based field work. For such areas important structural information regarding rift processes can be gleaned from magnetic data [*Modisi et al.*, 2000; *Grauch*, 2001] and Digital Elevation Models (DEM) [*Macheyeki et al.*, 2005; *Kervyn et al.*, 2006]. In this study we couple SRTM DEM data (which provides information on the surface morphology of the faults) with high-resolution aeromagnetic data (which provides information about the faults within the basement) to provide a three dimensional perspective of faults and fault patterns associated with ORZ. We use this information to: (1) examine fault linkage patterns in the ORZ, (2) investigate the development of border faults, and (3) demonstrate the utility of coupled SRTM DEM–high-resolution aeromagnetic data to provide important insights into the process of fault growth, linkage, propagation, and the development of border fault systems.

2. Okavango Rift Zone

[6] The Okavango basin in NW Botswana is located at the southern tip of the southwestern branch of the EARS (Figure 1). The rift lies within the Proterozoic Damaran mobile belt which is bounded by the Congo Craton to the NW and the Zimbabwe and Kaapvaal cratons to the southeast. The basement geology (Figure 2) in this area is mostly buried underneath 200–300 m of the Kalahari sediments and very few outcrops are exposed in the northern and southern part of the ORZ [*Modisi et al.*, 2000; *Kinabo et al.*, 2007]. Pre-Okavango geologic units include marls, clays, gravels, eolian sands, calcrete, and silcretes which define the 230-m-thick Cenozoic Kalahari beds. Carboniferous to Jurassic Karroo supracrustal sequences include sedimentary and volcanic rocks (Figure 2). A prominent feature is the west-northwest-trending 179 Ma Karoo dike swarm. One of the most important features present within the basement in this region are the relicts of the Mesoproterozoic to Neoproterozoic northeast trending NW Botswana Rift with a strike length of 600 km and a width of 250 km [*Key and Ayres*, 2000; *Modie*, 2000]. Rifting commenced in the Mesoproterozoic but the main phase of rifting occurred in the Neoproterozoic. The present-day Kalahari Suture Zone defines the southeastern margin of the rift. This fault zone has an extended history beginning as a major zone of Mesoproterozoic thrusting that was reactivated as a down to the northwest normal fault during the Neoproterozoic and then subsequently became the locus of thrusting during the

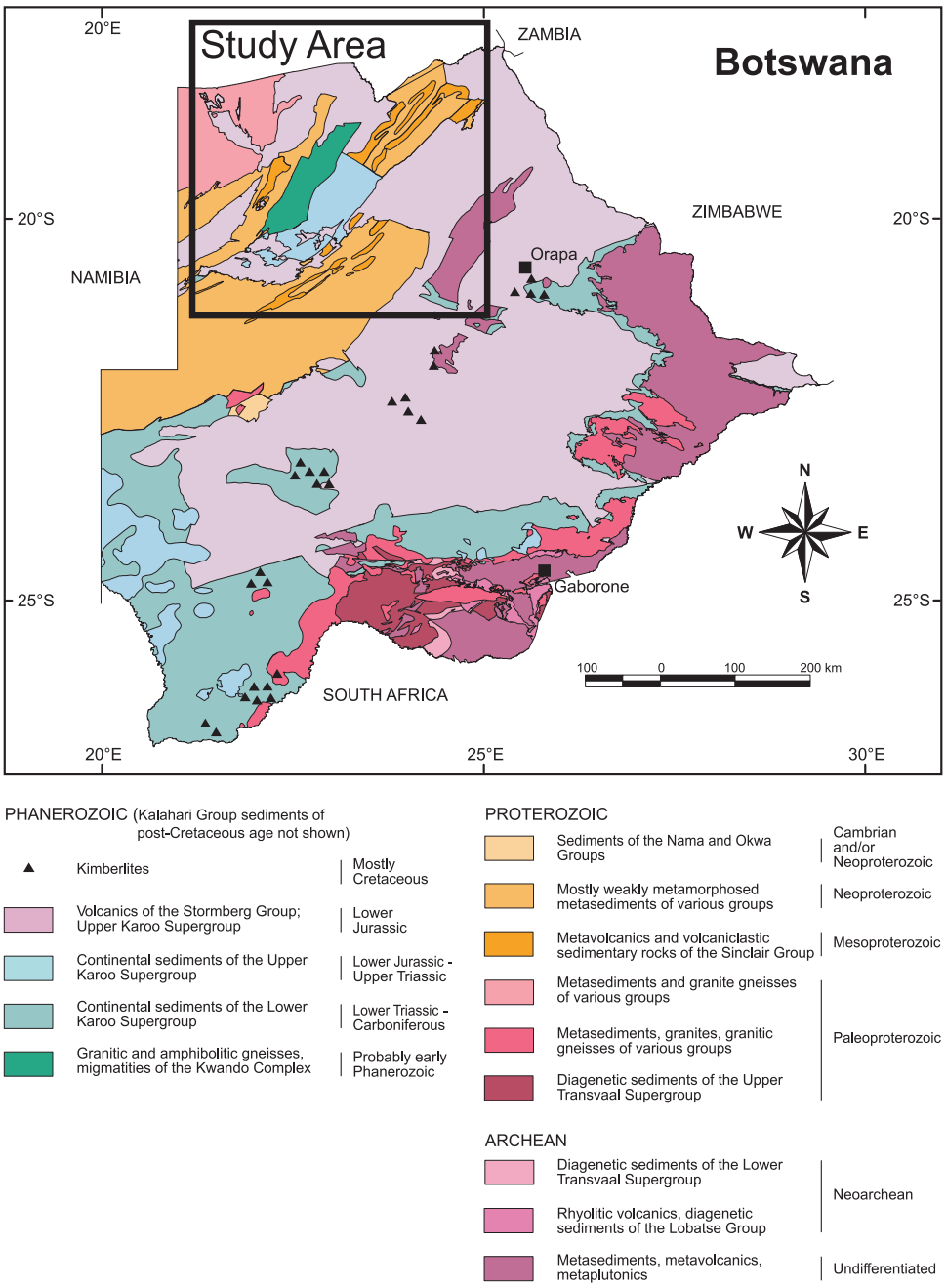

Figure 2. Geologic map of Botswana. Adapted from *Schlüter* [2006]. The study area is enclosed in the black box.

Damaran tectonism in the late Neoproterozoic to early Paleozoic [*Key and Ayres*, 2000]. The original northwest boundary of the rift is difficult to define because of overprinting during Damaran tectonism which intensifies to the northwest. Associated with the rift are a ~2 km thick pile of bimodal volcanic rocks of the Kwegbe Hills formation dated to be ~1.1 Ga [*Schwartz et al.*, 1996] which is overlain by 4–5 km of the Neoproterozoic Ghanzi Group sedimentary rocks. These sequences were subsequently folded during Damaran tectonism to define a pronounced northeast striking foliation readily visible in the aeromagnetic maps of the basement [*Key and Ayres*, 2000; *Kinabo et al.*, 2007]. Several models have been proposed for the origin of this rift including extension as a result of late stage orogenic collapse [*Kampunzu et al.*, 1998] or as a pull-apart basin formed in transtension as a result of late stage dextral shearing during the waning phases of the Mesoproterozoic continental collision [*Aldiss and Carney*, 1992]. The present-day ORZ is forming within the confines of this old rift and as discussed below, the older basement fabric is greatly influencing the development of faults and fault linkages associated with the ORZ.

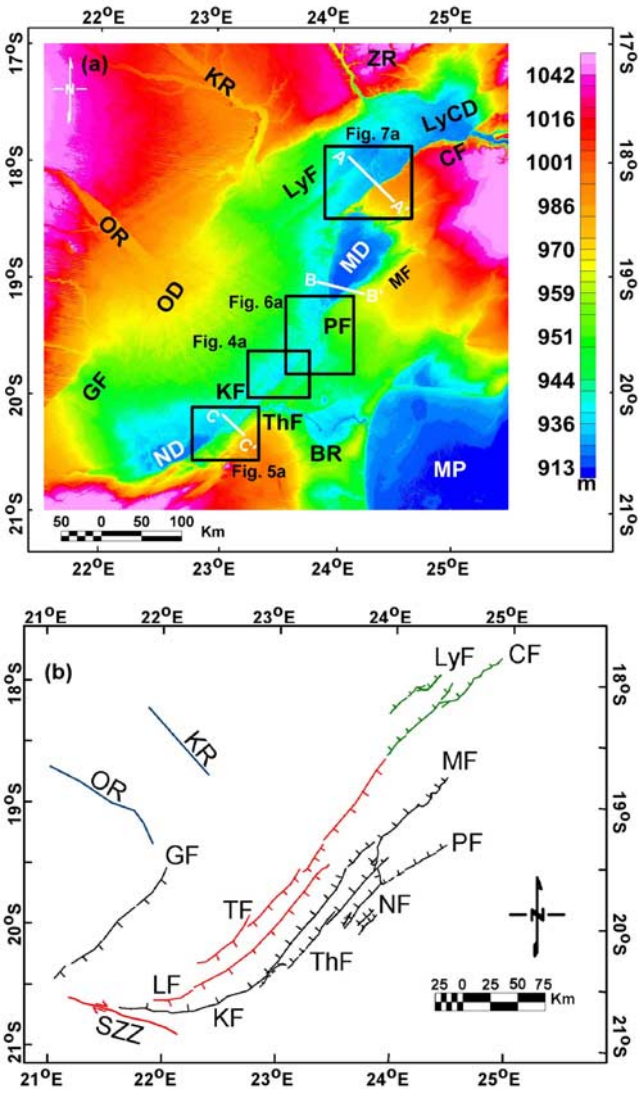

Figure 3. (a) SRTM DEM map of the Okavango Rift Zone showing major rift faults and depocenters. GF, Gumare Fault; KF, Kunyere Fault; ThF, Thamalakane Fault; PF, Phuti Fault; MF, Mababe Fault; CF, Chobe Fault; LyF, Linyanti Fault; MP, Makgadikgadi Pans; ND, Ngami Depression; LyCD, Linyanti-Chobe Depression; MD, Mababe Depocenter; ZR, Zambezi River; OD, Okavango Delta; OR, Okavango River; KR, Kwando River. The areas shown in boxes are shown in Figures 4–7, and white lines are profiles shown in Figure 8. (b) Structural map of the ORZ interpreted from aeromagnetic and SRTM DEM data (black lines). The faults in red were interpreted from aeromagnetic data, faults in green were interpreted from SRTM DEM, and faults in black were interpreted from both SRTM DEM and aeromagnetic data. The ticks on the faults indicate the fault dip azimuth. Symbols are same as in Figure 3a.

[7] Geological and geophysical investigations of the ORZ are sparse. *Fairhead and Girdler* [1969] and *Fairhead and Henderson* [1977] were probably the first scientists to recognize the southwesterly extension of the EARS into southern Africa including the area that is now known as the Okavango Rift Zone. Later, a micro-earthquake study conducted in this area in 1974 showed that seismic activity was largely associated with a set of en échelon Quaternary to Recent northeasterly striking normal faults [*Scholz et al.*, 1976] and led to the conclusion that the ORZ was an area of incipient rifting.

[8] The exact age of rifting in ORZ is not known. However, several lines of evidence can be used to constrain the age for initiation of rifting in ORZ. Rifting began after the 179 Ma Karoo dike swarm [*Le Gall et al.*, 2002] which are displaced by the rift faults (see Figure 4c). Paleoenvironmental records suggest that tributaries of the Okavango system promoted extensive wet and dry conditions beyond the Thamalakane and Kunyere faults circa and prior to 110 ka into the Makgadikgadi pans (Figure 3). However, ~41 ka vertical movements along rift-related faults caused impoundment of the Okavango River, cutting off water supply to the pans [*Ringrose et al.*, 2005] suggesting that the 41 ka age represents the best estimate for initiation of active rifting within the ORZ.

[9] More recently, *Modisi et al.* [2000] using high-resolution aeromagnetic data over the southern portion of the ORZ documented that the width of this rift is similar to that of the more mature basins of the EARS and that preexisting basement structures exert a major control over the rift development. *Kinabo et al.* [2007] using a more complete gravity and aeromagnetic geophysical database of the ORZ examined the full extent of the rift structures and confirmed a strong influence of preexisting basement fabrics on localization and development of rift related faults and established that the shape of the rift graben is synformal to half-graben. *Kinabo et al.* [2007] also described ten northeasterly trending rift faults associated with the ORZ including the Thamalakane, Kunyere, Linyanti, Chobe, Nare, Phuti, Lecha, Tsau, Gumare and Mababe and the east-southeasterly trending Sekaka Shear Zone (Figure 3). Surface mapping of these faults is difficult owing to widespread cover of eolian sand and colluvium and in addition drill hole information within the basin is sparse. Faults within the ORZ define a northeast trending rift zone that is ~400 km long and ~150 km wide (Figure 3). This study extends the investigation of the two previous studies [*Modisi et al.*, 2000; *Kinabo et al.*, 2007] by focusing on the details of fault growth, linkage, and propagation, and the development of border faults during the early stages of continental rifting.

3. Data Acquisition and Processing

3.1. Shuttle Radar Topography Mission, Digital Elevation Model (SRTM DEM)

[10] The February 2000 Shuttle Radar Topography Mission (SRTM) was a joint international project between the United States National Geospatial-Intelligence Agency (NGA) and the National Aeronautics and Space Administration (NASA), and the German and Italian Space Agencies. SRTM DEM is distributed by NASA's Jet Propulsion

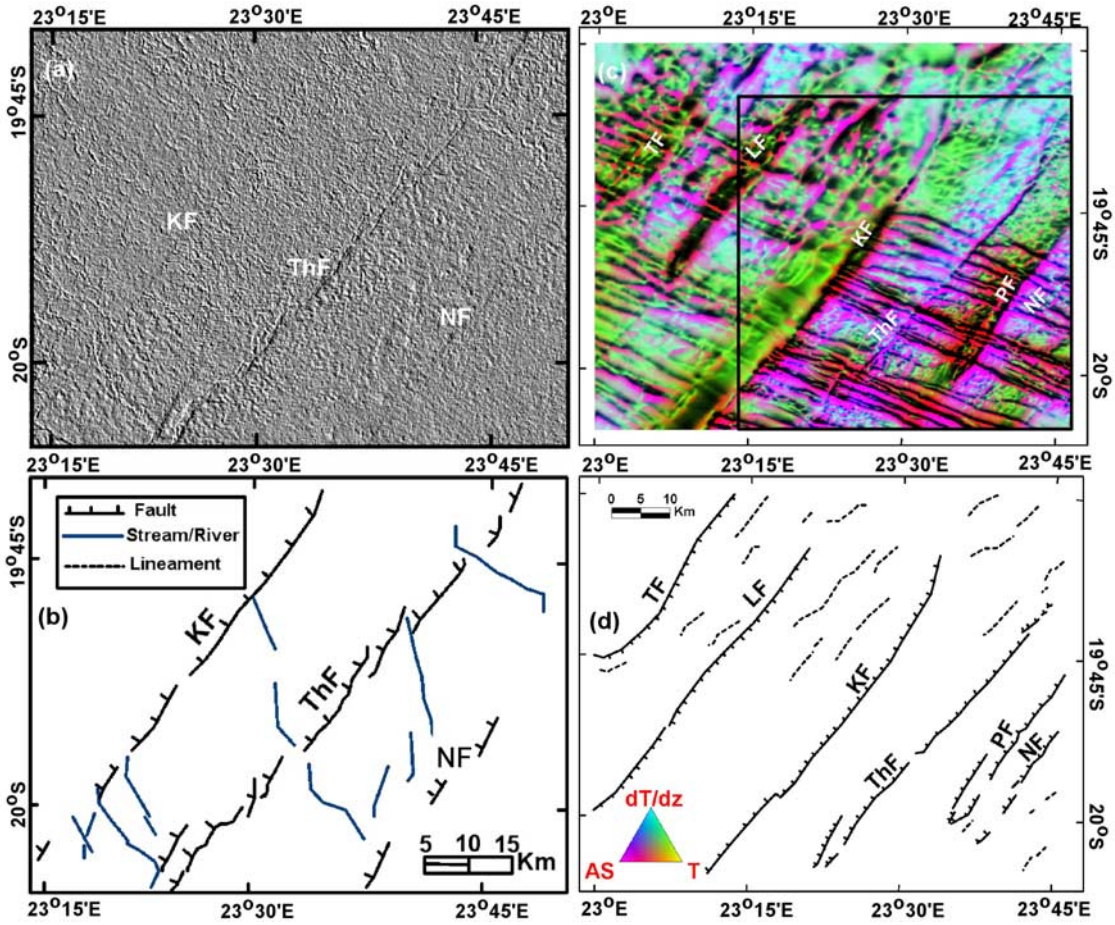

Figure 4. (a) Hill shade SRTM DEM map showing isolated segments along the Kunyere Fault and overlapping en échelon fault segments along the Thamalakane Fault. Illumination is from the NE. Refer to Figure 3a for the area location. (b) Structural interpretation map of Figure 4a. (c) Ternary magnetic anomaly map showing continuous hard linked segments along the Kunyere and the Thamalakane faults. The area shown in Figure 4a is enclosed in a black box. (d) Structural interpretation map of Figure 4c. Fault labels are same as in Figure 3a.

Lab (JPL) in 1° × 1° tiles. Two types of SRTM data are available: one arc data (SRTM-1, 30 m X-Y resolution); and three arc data (SRTM-3, 90 m X-Y resolution and ±30 m root mean square error z accuracy). Only SRTM 3 data are available for Africa and, therefore, are used in this study. Data were analyzed using ENVI. Data scenes were combined to form a mosaic and registered using image-to-image technique [*Chen and Lee*, 1992]. Visual interpretations of SRTM DEM are shown in the form of structural maps illustrating the strike, dip direction, and spatial distribution of these faults and related structures (Figures 4b, 5b, 6b, and 7b). Topographic profiles were extracted from SRTM DEM data from selected areas to document the morphology associated with surface rupture of the rift faults. Three topographic profiles (Figure 8) were extracted across the selected lineaments to demonstrate a consistent existence of fault scarps (the profiles are 4–14 km apart). A moving average of 20 data points was applied to filter out above ground features such as trees and boulders. Throughout our discussion we will use DEM to represent SRTM DEM.

3.2. Aeromagnetic Data

[11] The aeromagnetic data were acquired in 1996 under the direction of the Geological Survey of Botswana. The flight elevation was 80 m along north-south lines with spacing of 250 m and tie lines were east-west (spaced 1.25 km apart). The international geomagnetic reference field was removed and data were gridded using a grid cell size of 62.5 m and the minimum curvature technique [*Briggs*, 1974; *Swain*, 1976]. The grid cell size provides an estimate of the resolution of the aeromagnetic data. Minimum curvature gridding is accomplished by fitting the smoothest possible surface to data values. First and second vertical derivative filters were applied to the total field magnetic data in order to enhance shallow seated features of the rift and the basement. Ternary maps were

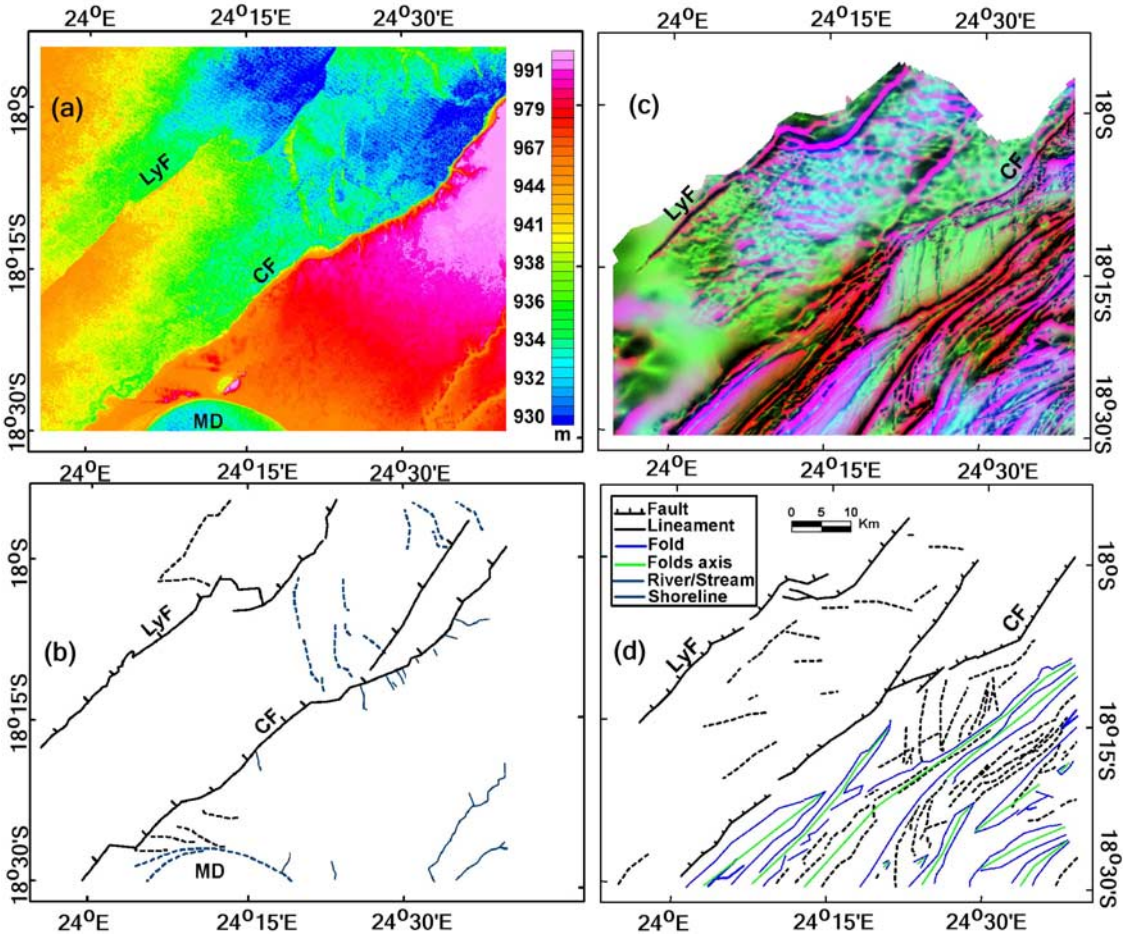

Figure 5. (a) SRTM DEM map showing hard linkage along the Linyanti and Chobe faults. Refer to Figure 3a for the area location. (b) Structural interpretation map of Figure 5a. (c) Ternary magnetic anomaly map of the same area. Note the folds in the basement as revealed by a ternary map. (d) Structural interpretation map of the Figure 5c. Labels are the same as in Figure 3a.

prepared in order to enhance basement structural features such as dikes, faults, fractures, and folds. A ternary diagram is a map made by combining color attributes of three separate data sets; in this study optimum enhancement of basement structures was obtained by plotting the total magnetic field, vertical derivative, and analytical signal data into one color map (Figures 4c, 5c, 6c, and 7c). The ''analytical signal'' is the square root of the sum of the squares of the derivatives in three orthogonal directions as shown in the equation below

$$\textit{Analytical signal} = \sqrt{\left(\frac{\partial^2 T}{\partial x^2} + \frac{\partial^2 T}{\partial y^2} + \frac{\partial^2 T}{\partial z^2}\right)}. \qquad (1)$$

[12] The analytical signal is useful in locating the sources of magnetic bodies. Structural interpretation maps were made from the ternary maps by tracing lineaments and by defining boundaries between domains of distinctly different magnetic character (Figures 4d, 5d, 6d, and 7d). Depths to the top of magnetic sources calculated from 3-D Euler deconvolution presented by *Kinabo et al.* [2007] were used to determine the vertical displacements along the faults. Parameters used for the depth estimates included a structural index of 1 for dikes, which were used as displacement markers because of their pervasiveness in the area and their crosscutting relationship with the rift faults. We defined an error limit of 5% for the depth and horizontal positions thereby limiting solutions. Vertical throws across faults were estimated by taking the difference in depth between two segments of the dike displaced by faults (Figure 9). As documented by *Modisi et al.* [2000], Euler solutions depth estimates across the fault zones are consistent with available borehole data depths within the rift zone.

3.3. Interpretation and Mapping of Lineaments

[13] Surface mapping of faults within the ORZ is difficult owing to widespread surficial cover and weathering of the rocks cut by faults. In most of the basin, fault zones are easily eroded and commonly covered by calcrete. Hence, we relied on the DEM to map faults, using abrupt changes in color or tonal patterns, subtle topographic scarps, linear

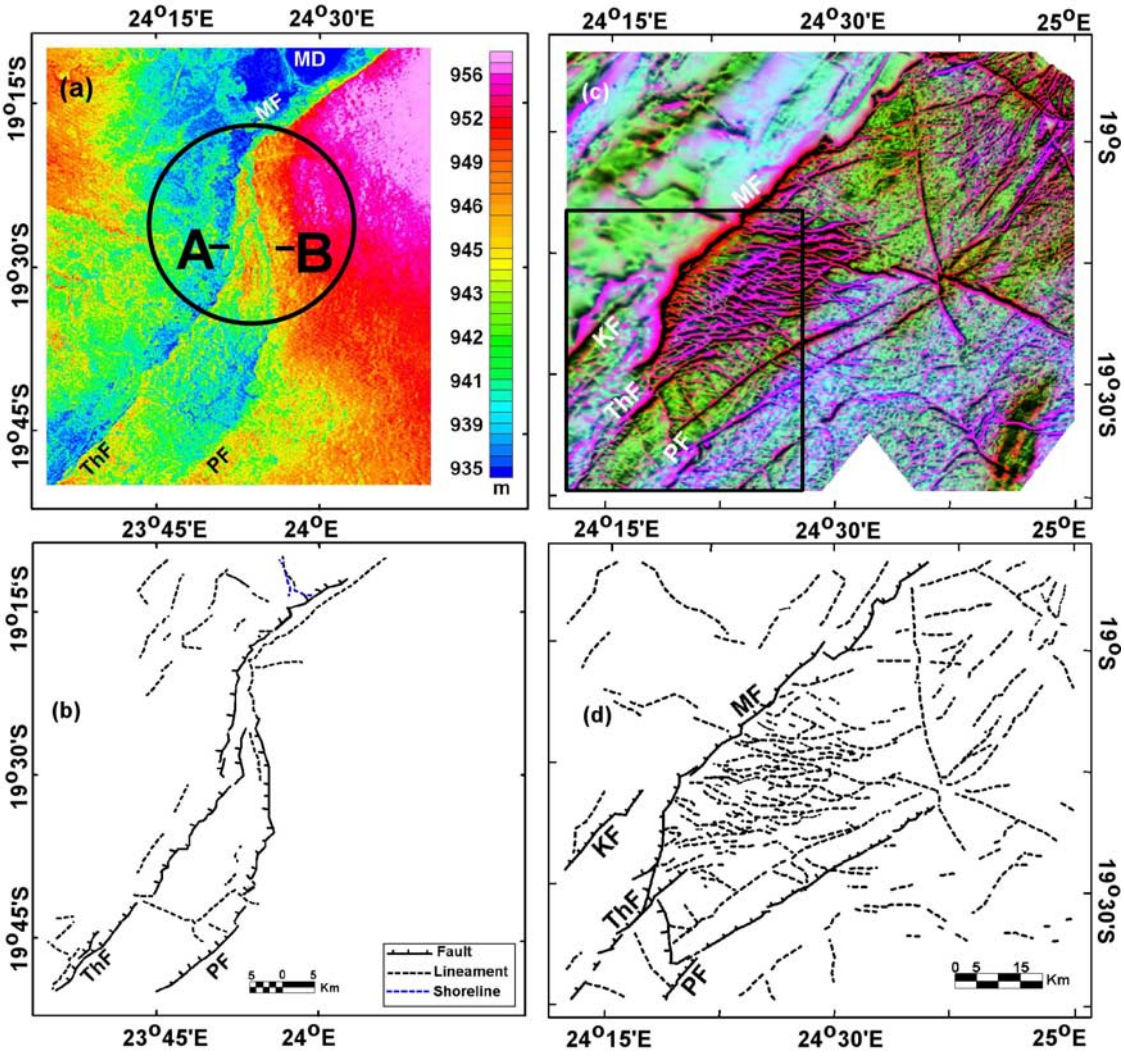

Figure 6. (a) SRTM DEM image showing linkage of the Thamalakane and Phuti faults to the Mababe fault. Refer to Figure 3a for the area location. The black circle encloses A (channel A) and B (channel B) which occupy fractures linking the Thamalakane Fault to the Mababe Fault and the Phuti Fault to the Mababe Fault, respectively. (b) Structural interpretation map of Figure 6a. (c) Ternary magnetic anomaly map showing hard linkage along the Mababe Fault. The black box shows the area shown on Figure 6a. (d) Structural interpretation map of Figure 6c. Labels are the same as in Figure 3a.

drainage patterns, and/or isolated exposures of mapped units that are offset vertically. To confirm that the topographic features mapped from the DEM are fault related rather than fluvial erosional or depositional structures, slope convexity analysis was performed [e.g., *Nash*, 1986]. Slope convexity is a measure of gentleness of a slope. In this analysis fault related slopes return a value of zero, depositional slopes a value of +1, and erosional slopes a value of −1. The slope convexities of suspected fault scarps were then analyzed by extracting topographic profiles across the suspected fault scarps from the DEM data. In addition, a close spatial correspondence between the position of scarps on the DEM and the position of faults in the basement as mapped using the aeromagnetic anomalies was used to check for consistency in interpreting topographic scarps as being fault related (e.g., Figures 4 and 5). Other pronounced lineaments on the DEM, presumably corresponding to fractures, dikes, and in other locations stream channels, were noted and mapped. Rose diagrams were constructed using the azimuth of these lineaments to facilitate evaluation of spatial correlations and interpretation of these features (Figure 10).

[14] Several map enhancements and analytical techniques as discussed above were applied to the aeromagnetic data to help understand fault parameters and their aeromagnetic expressions. In the high-resolution aeromagnetic data, faults were identified as dominantly linear to slightly curving lineaments that typically have very pronounced analytical signals and by the presence of: (1) abrupt changes in the magnetic character or fabric, (2) linear clusters of Euler solutions, (3) the magnitude of the vertical derivative,

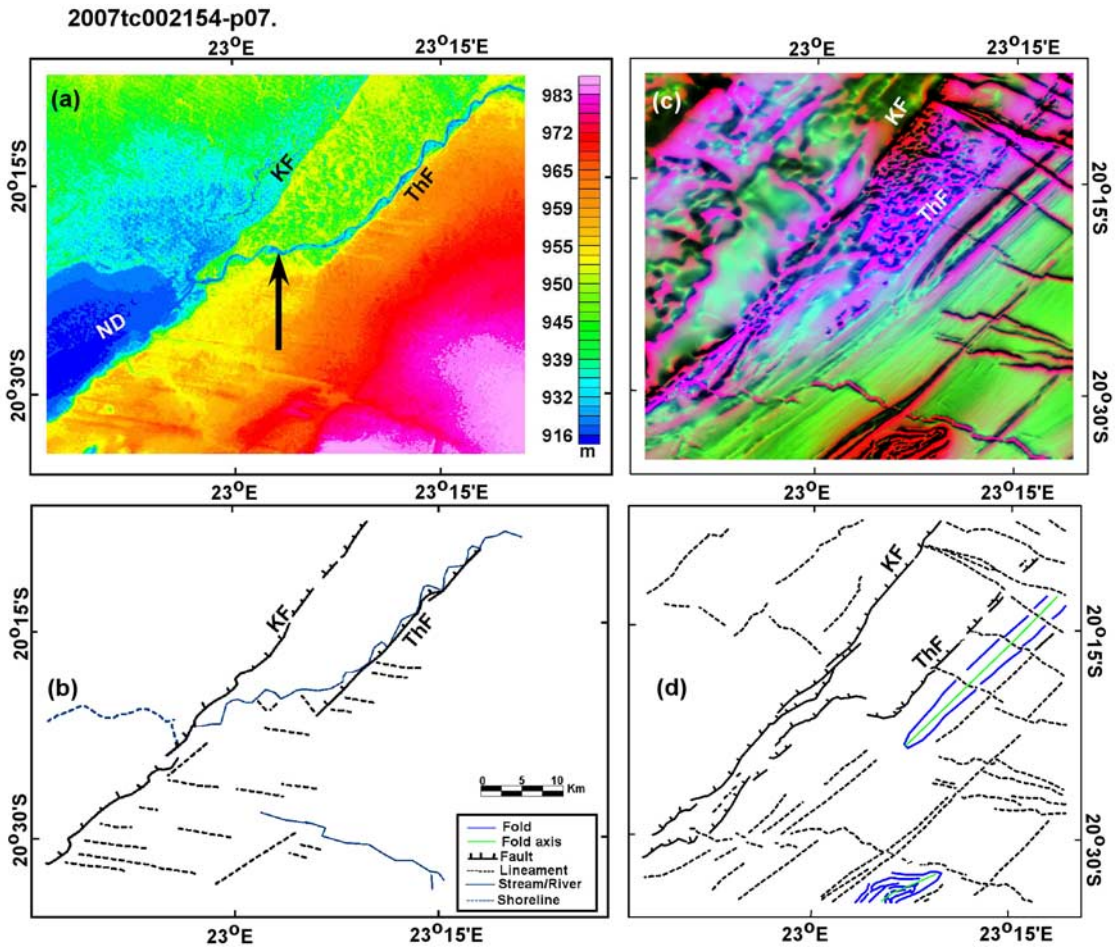

Figure 7. (a) SRTM DEM map showing a connecting fault (shown by an arrow) linking the Kunyere and Thamalakane faults. Refer to Figure 3a for the area location. (b) Structural interpretation map of Figure 7a. (c) Ternary magnetic image of the same area as Figure 7a. (d) Structural interpretation map of Figure 7c. Labels are the same as in Figure 3a.

(4) magnetic intensity, and/or by (5) truncation of prominent magnetic anomalies known to be related to the ESE-WNW Karroo dike swarm [*Modisi et al.*, 2000]. The change in the magnetic intensity of the dikes across the linear magnetic anomalies indicates a difference in magnetic contrast across the fault. For example, on Figure 4c the ESE-WNW trending linear anomalies (purples) associated with the Karoo dikes is clearly visible on the east side (up-thrown block) of the Kunyere Fault. However, across the fault, dike anomalies are more subtle and of lower intensity (greens and blues) consistent with this being the down-thrown block; that is, the depth to the top of the magnetic source is deeper resulting in the lower amplitude of the magnetic anomalies (see Figure 9). Other pronounced lineaments in the aeromagnetic data set, presumably corresponding to dikes, basement fractures, lithologic layering, and the trace of fold axes, were noted and mapped. The correspondence of mapped linear magnetic anomalies to surficial evidence of faulting across the area is the primary evidence that the linear anomalies represent aeromagnetic expressions of faults. In map view, these linear anomalies show patterns typical of extensional faulting, such as anastomosing (e.g., Chobe Fault, Figure 5c) and en échelon segments (e.g., Linyanti Fault, Figure 5c). Additionally, linear anomalies associated with faults have amplitudes on the magnetic map that commonly range from 200–600 nT with widths of 150–200 m.

[15] Rose diagrams were constructed using the azimuth of these lineaments (Figure 10). The location of suspected fault boundaries, and other mapped lineaments in the aeromagnetic map were then qualitatively compared with fault scarps and lineaments identified on the DEM to evaluate their degree of spatial correlation.

4. Results

[16] Structural maps constructed from a combined analysis of topographic lineaments as depicted on the DEM data and magnetic lineaments in the buried basement rocks as depicted in the aeromagnetic data are shown in Figures 4–7

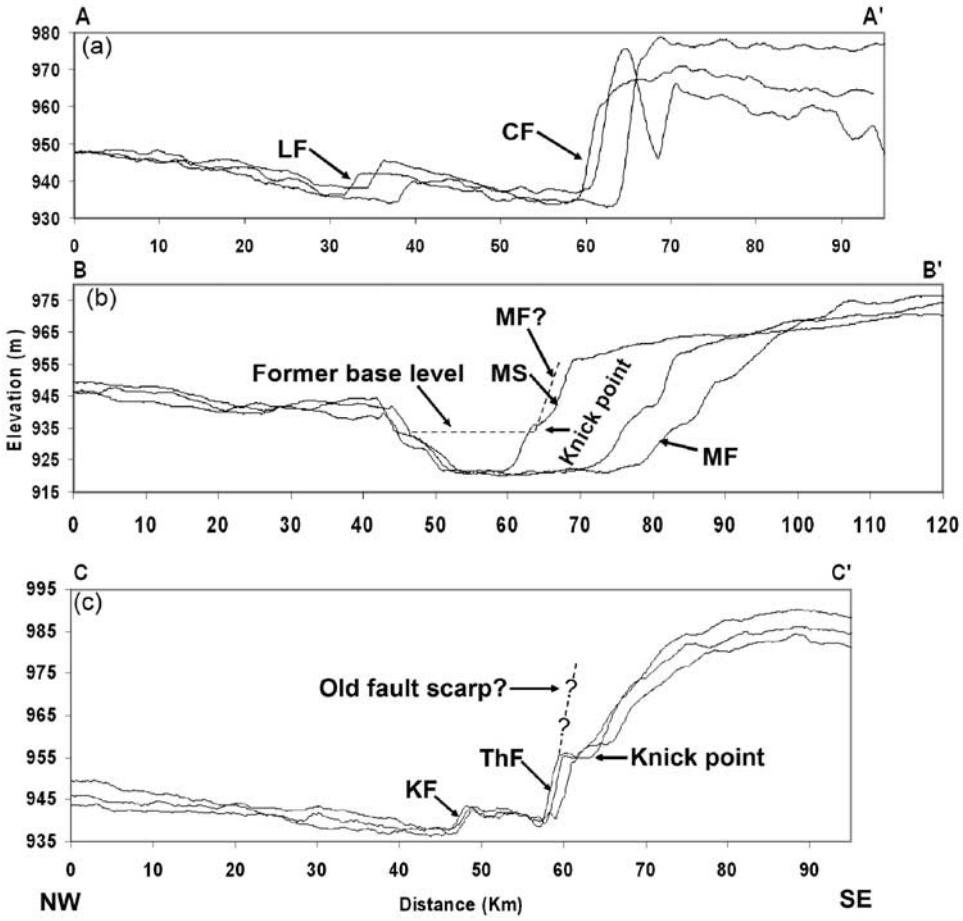

Figure 8. Profiles showing scarps in the ORZ. (a) Profiles A-A′ along the Linyanti Fault (8 m) and the Chobe Fault (33–44 m); profile are ~10 km apart. (b) Profile B-B′ along the Mababe Depression, Mababe Scarp (12–18 m); profiles are >13 km apart. (c) Profiles C-C′ along the Kunyere Fault (6 m) and the Thamalakane Fault (18 m); profiles are >4 km apart. See Figure 3a for the location of the profiles. The annotation on the bottom of profile C-C′ and to the left of profile B-B′ apply to all profiles. MS, Mababe topographic Scarp; other labels are the same as in Figure 3.

for selected regions of the ORZ. The ORZ is defined by eleven recognized major fault systems; they are the Chobe, Linyanti, Mababe, Phuti, Nare, Thamalakane, Tsau, Gumare, Lecha, and Kunyere Fault Zones, and the Sekaka Shear Zone (Figure 3). The physical characteristics of the faults (e.g., total lengths, throw, scarp height, linkage style) as independently determined from the DEM and from the aeromagnetic maps are summarized in Table 1. Our observations are as follows.

4.1. Fault Throws Versus Scarp Heights

[17] Comparison of the throw on the fault (as measured on the aeromagnetic maps) to the height of the fault scarp (measured on the DEM) reveals three distinct classes of faults within the ORZ (Table 1). The first class of faults are those in which the throw and fault scarp height are approximately equivalent. The Gumare Fault with vertical throw of ~17 m and scarp height of 20 m is the only example of this fault class. The second class of faults comprises those that exhibit significant throw on the basement surface but no topographic expression (Figure 4). Examples of these faults include the Lecha and Tsau faults. The Lecha Fault is 200 km long with vertical throw range of 56–163 m and the Tsau Fault is 100 km in length and has a vertical throw of 43–130 m. These faults occur toward the interior of the rift basin (Figures 3 and 4). The third class of faults exhibit large throws on the basement but relatively subdued fault scarps. For example, the Kunyere Fault has a throw on the basement of ~232–334 m yet the fault scarp is only 6 m high (Figure 8c). The fourth class of faults exhibit large throws and significant faults scarp heights (i.e., >10 m). Examples of these faults include the Chobe Fault, the Mababe Fault, and the Thamalakane Fault (e.g., Figure 8).

4.2. Fault Heave

[18] Lateral offset of individual dikes of the Karroo Dike Swarm potentially can provide a sense of the relative magnitude of the heave along these faults, especially if

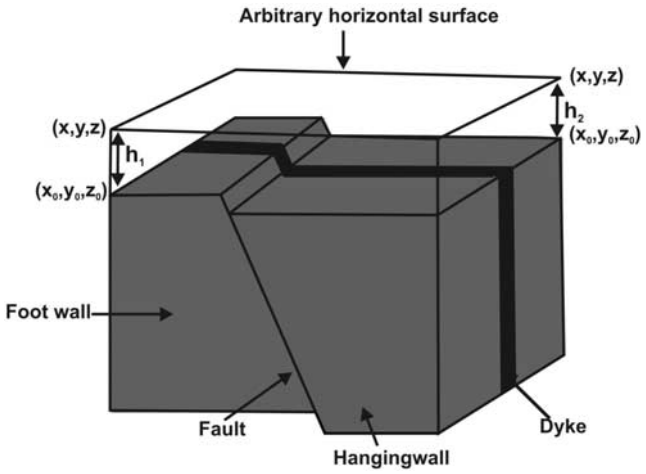

Figure 9. Schematic diagram illustrating the use of dikes as markers for estimating faults vertical displacement (throw) using 3-D Euler deconvolution technique. Fault throw across the fault shown on the diagram is given by h_2-h_1. Note that the sediments have a near-zero magnetic susceptibility and therefore they are not a factor in estimation of the fault throw.

the dikes have near vertical dips. In general, the traces of the dikes show little horizontal offset, indicating that the majority of the movement along the faults is dip-slip in nature [*Modisi et al.*, 2000]. Locally, faults can exhibit evidence for a strike-slip component. For example, along the Thamalakane Fault the magnetic expression of the Karroo Dikes display a right lateral separation ($\leq$1 km; Figure 4c). However, to the south similar lineaments display a left-lateral sense of displacement along an unnamed fault in the basement (Figure 7c). It is unknown whether this reflects a true-slip component or an apparent slip due to locally some dikes having dips less than 90°.

4.3. Fault Segmentation (Surface Versus Basement Expression)

[19] On the DEM, fault systems commonly comprise several individual fault segments readily recognizable as discrete topographic scarps. Measured at the surface, segments within fault systems are typically 3–25 km in length. Within a particular fault zone, the style of fault linkage between the different fault segments can be interpreted from the topographic patterns of the fault scarp lineaments on the DEM. Fault segmentation patterns present in the ORZ include: (1) underlapping (discrete or nonoverlapping) fault segments as in the case of the ~3- to 8-km-long segments along the Kunyere Fault (Figures 4a and 4b) where the spacing between the fault segments is in the range of ~2.5–3 km, (2) overlapping of right stepping en échelon fault segments that are ~3–15 km in length observed along the Thamalakane Fault (Figures 4a and 4b), (3) hooking or touching of segment tips, exemplified by the Linyanti Fault (Figures 5a and b), and (4) along-strike bending of fault segments (fused segments) as observed along the Mababe Fault (Figures 6a and 6b) and Gumare Fault (Figure 3).

[20] The degree and style of fault segmentation of individual fault zones characterized from the topographic ex-

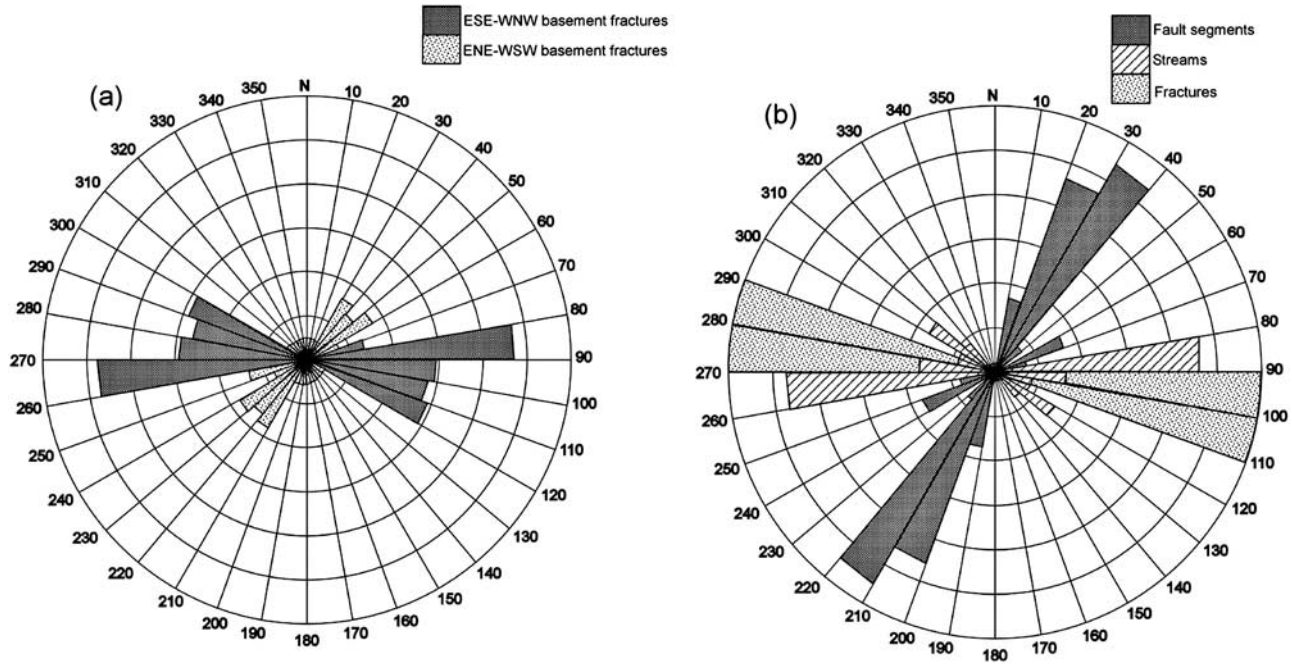

Figure 10. Rose diagram showing the orientation of faults, fractures, and streams in the ORZ. (a) Azimuth of fractures from the area shown on Figure 6c. (b) Azimuth of fractures, faults and stream in the area shown on Figure 7a.

Table 1. Physical Characteristics of Selected Faults From the Okavango Rift Zone[a]

Fault Name	Topographic Characteristics		Basement Characteristics		
	Digital Elevation Model (DEM)			Aeromagnetic Maps	
	Fault Length (km)	Scarp Height (m)	Convexity[b]	Fault Length (km)	Fault Throw (m)
CF	~260	33–44	−0.05–0.02	~150	ND
GF	~168	~20	−0.02–0.02	~180	~17
KF	~172	~6	−0.02–0.02	~325	232–334
LF	NTE	NTE	NTE	~200	56–163
LyF	~150	~8	−0.03–0.02	~75	ND
MF	~96	12–18	−0.03–0.01	~100	~521
NF	NTE	NTE	NTE	~25	~71
PF	~38	~2	0.01–0.02	~65	~18
ThF	~154	~18	−0.03–0.04	~100	~80
TF	NTE	NTE	NTE	~225	43–130

[a]NTE, no topographic scarp; ND, not determined.
[b]Estimated from SRTM DEM.

pression of the fault scarps on the DEM can differ from that determined from the expression of the same fault in the basement on the aeromagnetic map. For example, the Kunyere Fault is composed of four segments that are 3–8 km long on the DEM whereas on the aeromagnetic map it is a continuous fault composed of possibly two segments that are 20 and 50 km in length (Figure 4). The DEM expression of the Thamalakane Fault (Figures 4a and 4b) is characterized by en échelon right stepping segments that are 3–15 km long while the aeromagnetic expression of the same fault is characterized by fewer relatively longer (~20–30 km in length) fault segments (Figures 4c and 4d).

5. Discussion

5.1. Fault Characteristics

[21] All the faults mapped on the aeromagnetic maps, with the exception of the Lecha and Tsau Faults, have topographic scarps associated with their surface expressions (e.g., Figure 4 and Table 1). The lack of surface expression for the Lecha and Tsau basement faults may indicate (1) that these are much older faults that for some reason have remained inactive during the extensional tectonic regime associated with the ORZ, (2) these faults are active but lack sufficient energy to rupture the surface (i.e., blind normal faults), or (3) that these basement faults were active during the early stages of ORZ rifting, but have now been concealed by rapid sedimentation associated with Okavango alluvial fan deposits. We suggest the final possibility as the more likely alternative as below we discuss that the rift is widening and abandoning interior faults as it matures. For many faults, the scarp heights are significantly smaller than the fault throw values calculated from the 3-D Euler deconvolution solutions (Table 1). The discrepancy is as much as 500 m along the Mababe Fault. We offer the following possible explanation for these differences. Extended fault histories comprises multiple displacement events coupled with ongoing sedimentation will result in differences between the throws on the basement and the fault scarp height. In this case, the throw on the basement records the time integrated displacement over the life of the fault, whereas, the height of the fault scarp will record only the more recent movements on the fault. Thus, higher sedimentation rates from the Okavango River compared to the vertical movement along still active faults can lead to partial or complete burial of older fault scarps. Conversely, faults that were once active and have since become dormant or relatively inactive will have fault scarps that are diminished by even moderate to low sedimentation rates. Recent seismic events along several of the major rift faults support the higher sedimentation rates scenario [*Scholz et al.*, 1976].

[22] Within the ORZ, major fault zones and their segments have orientations that parallel the structural fabric of the basement emphasizing the role of preexisting structures on the development of rift faults [e.g., *Ring*, 1994]. This strength anisotropy in the basement greatly influenced the location and orientation for brittle failure. For example, the low displacement to length scaling relations observed for these faults may to a large extent reflect a reduction in the stress required to produce failure and laterally propagate faults along these preexisting planes of weakness. Thus we suggest that in areas of continental rifting where older basement structures are oriented favorably to exert a strong influence on fault development, normal faults with seemingly anomalous strike lengths of 100 km [e.g., see *Foster et al.*, 1997; *Ebinger et al.*, 1997] may appear early in the development of the rift. In addition, comparison of the throw on the basement surface with the throw on the topographic fault scarp demonstrates that many of the faults have extended histories. Most of the faults suggest evidence for multiple episode of faulting with concomitant sedimentation along the down thrown block and erosion of the fault scarps. The presence of terraces in the Mababe and Thamalakane fault scarps subdivides the profiles into multiple upper and lower scarps (Figures 8b and 8c). The topographic slope on the scarp above the terrace has been modified by erosion. The topographic slope on the scarp below the terrace does not appear to have been significantly modified by erosion (Figure 8c). We interpret the topographic terraces separating the upper and lower scarps to reflect retreat of the

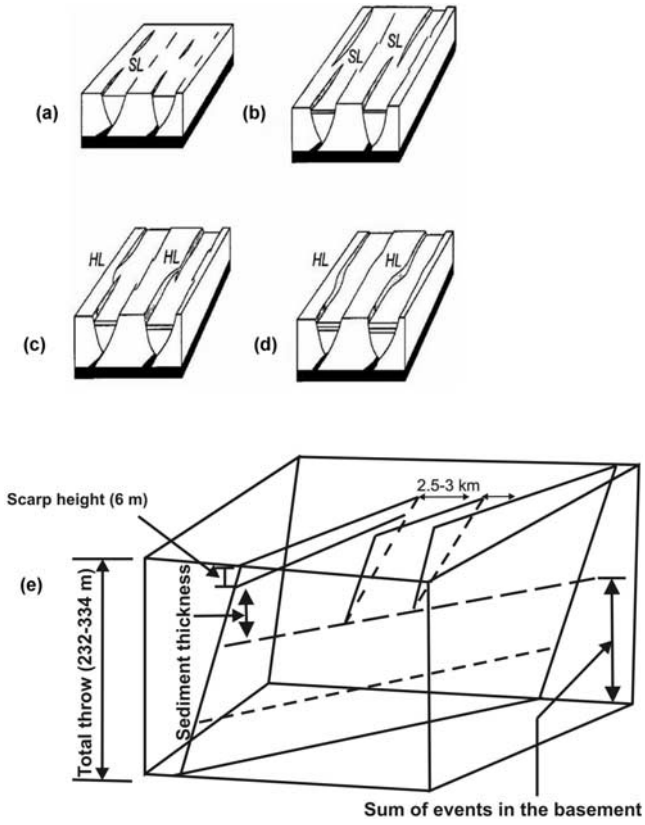

Figure 11. (a) Model showing fault growth and linkage in a progressively increasing stress extensional environment. Modified from *Le Calvez and Vendeville* [2002]. (b) En échelon segments at the surface may be twists connected to the same fault plane at depth as exemplified by portions of the Kunyere Fault and Thamalakane Fault in Figure 4.

fault scarp as a result of erosion during the hiatus between episodes of faulting. This requires the multiple episodes of faulting to have been sufficiently recent and spaced closely enough that erosion has not removed the topographic evidence of the older displacement. Alternatively, the terraces may also reflect changes in local base level (Figure 8b), which is consistent with the presence of well marked former shorelines of Lake Mababe (Figure 3). The extent to which changes in local base level is in turn influenced by faulting remains to be constrained. Thus, older faults that have established long fault traces as a result of multiple episodes of faulting and through linking of fault segments may exhibit topographic scarps with lower than expected relief as a result of: (1) the height of the topographic fault scarp reflects only the most recent displacement event that ruptured the surface, (2) since the last displacement, the height of the fault scarp has been reduced by sedimentation, (3) the height of the fault scarp has been reduced by erosion, and/or (4) these faults propagate laterally to much greater extents than predicted from fault length fault throw scaling relationships because of the relative ease by which preexisting weaknesses in the basement terranes fail.

5.2. Fault Growth and Propagation

[23] Integrating the results from the two data sets allow us to better evaluate the three dimensional geometry of the fault planes, and therefore the growth of faults through fault linkages based upon the patterns of fault scarps in the DEM and fault traces in the aeromagnetic maps [e.g., see *Walsh et al.*, 2003]. For example, the traces of the Thamalakane and Kunyere faults are segmented on the DEM map but are continuous on the aeromagnetic map (Figure 4). The faults initiate at depth nucleating on preexisting planar weaknesses within the basement as long continuous faults. As the leading edge of the propagating fault plane approaches the topographic surface, twists similar to those which form along the margins of joints, develop and rupture the surface (Figure 11). These twists will appear as en échelon fault segments on the DEM and could be erroneously interpreted as discrete fault planes related by soft linkage even in the basement if only the DEM data were available for interpretation. *Walsh et al.* [2003] also present examples where segmented faults, when viewed on two dimensional maps could be considered as separate isolated faults, but in three dimensions can be shown to be related to a single fault that formed relay zones as the fault propagated upward toward the free surface (supporting the coherent model of *Walsh et al.* [2003], where a developing en échelon fault at the surface is linked at depth to form a single fault).

[24] With these cautions in mind, the results of the combined aeromagnetic and DEM investigations are consistent with a model for fault evolution beginning with exploitation of preexisting weakness in the basement by short discrete fault segments (3–25 km long) which propagate and eventually merge to form long continuous fault segments (~25–325 km long). Current models for fault growth and development suggest that faults grow as a result of formation of first soft linkages then hard linkages between small originally isolated fault segments [*Peacock and Sanderson*, 1991; *Trudgill and Cartwright*, 1994; *Dawers and Anders*, 1995; *Cowie*, 1998b] (although, see *Walsh et al.* [2003] for an alternative model). Within a regional stress field, which fault segments will remain active and eventually link together to grow and, which will eventually become inactive to a large extent is dependent upon the spatial location of fault segments with respect to the stress shadows of the neighboring fault segments [*Cowie*, 1998b]. Faults that are optimally oriented with respect to their neighbors will be more active and lengthen faster than faults that are positioned within the stress shadows of other faults. This creates both a positive and negative feedback between faults leading to the development of larger fault systems by the linking of the optimally favored fault segments at the expense of the other faults (e.g., this scenario is evident between the Kunyere and Thamalakane faults, Figure 7 (see discussion below)). The active fault segments initially interact through soft linkages which are characterized by underlapping segments that with increased stress continue to propagate and eventually overlap to form relay ramps. Further increase of stress leads to the development of hard linkages, which is marked by development of connecting faults across the relay ramp,

and finally destruction of the relay ramp by the connecting faults resulting in complete fusion of the originally isolated segments by a lateral ramp or transfer fault [e.g., *Peacock and Sanderson*, 1991] (Figure 11). The scaling relationship between displacement (D) and length (L) seen for individual fault segments $D_{max} \sim(0.009-0.014)L$ is maintained over the length of fault systems and reflects the material strength properties of the fractured rock [*Dawers et al.*, 1993]. *Dawers and Anders* [1995] used this scaling relationship to suggest that the coalescence of smaller fault segments as a mechanism to redistribute large localized accumulations of strain (especially in the regions of emerging fault linkages) over the entire fault system is an important driving force for fault growth.

[25] Using this model we interpret that faults in ORZ are at different temporal stages of fault evolution. Linkage of smaller fault segments within the same fault zone can be observed on both the DEM and aeromagnetic maps. The Linyanti Fault preserves evidence for a hard linkage between two fault segments by hooking. In both the DEM and the aeromagnetic map, the traces of each of these faults bend toward each other to overlap without merging (Figure 5). To the southeast of the Linyanti Fault, the topographic trace of the Chobe Fault also displays the relicts of a system of right-stepping en échelon segments that have essentially merged into a continuous fault scarp. In the aeromagnetic map the linkage between two overlapping fault segments along a right-handed step-over forming the current Chobe Fault is clearly marked by a zone of tightly spaced anastomosing faults and fractures. To the northwest of this hard linkage, the trace of the former fault tip is well marked as a magnetic high but with little displacement between the two sides of the fault.

[26] Evidence for linkage between major fault zones which are subparallel to the rift can also be seen on the DEM and aeromagnetic maps. For example, different styles of fault linkages between the Kunyere Fault and the Thamalakane Fault can be observed along strike between these two fault systems (Figure 3). Beginning at the southern end of the ORZ, within the Ngami Depression the linkage is accentuated on the DEM by a bend and then by abrupt deflections in the orientation of the main channel of the Thamalakane River, which flows along the Thamalakane Fault scarp (Figures 7a and 7b). Here the main Thamalakane Fault scarp peters out into a zone of less well pronounced, but abundant -east-west lineaments. On the aeromagnetic map the trace and throw along the Thamalakane Fault decreases along strike to the south. Here the Kunyere Fault zone is characterized by multiple fault segments, one of which hooks eastward toward the Thamalakane Fault (Figures 7c and 7d). We interpret this to represent a soft linkage along a relay ramp between these two normal faults [e.g., see *Cartwright et al.*, 1995]. Along strike to the north these two fault zone remain distinct (Figure 4). On the DEM the more subtle trace of the Kunyere Fault tip dies out to the north, whereas, the Thamalakane Fault scarp remains well defined and segmented (see also Figures 6a and 6b). On the aeromagnetic map the trace and displacement along the Kunyere Fault also diminishes toward the northern tip of this fault. Additionally, the throw on the basement is significantly larger than that observed for the fault scarp (Table 1), again potentially indicating waning displacement along this fault and/or increased sedimentation. We interpret the apparent inactivity on this segment of the Kunyere Fault to its location now residing within the strain shadow of the Thamalakane Fault [e.g., see *Cowie*, 1998b] as a result of linkages that formed between these two faults as part of the process of fault piracy described later in this paper. In the basement, the trace of the Thamalakane Fault exhibits fewer segments than on the DEM. To the north, the DEM for this area shows the Thamalakane and Phuti faults both converging into the Mababe Fault as each fault system hooks toward the other (Figures 6a and 6b). However, the convergence of these fault zones by hooking is not obvious on the aeromagnetic anomaly maps even thought it appears to be present (Figures 6c and 6d). Instead, the trace of the Thamalakane Fault zone overlaps with that of the Mababe Fault before ending in a diffuse zone of abundant lineaments that we interpret as fractures and minor faults (Figure 6). The Phuti Fault also appears to continue to the north and an additional fault, not recognized in the DEM, parallels the trace of this fault. The soft linkage of these faults is occurring across this diffused strain zone. It is striking that locally abrupt changes in the drainage pattern of the river channel define segments whose orientations also closely coincide with the orientations of fractures and faults (Figure 10).

[27] The results of this study extend the initial findings of *Kinabo et al.* [2007] and help clarify the development of rift faults on the basis of the observations from both the basement and the surface geomorphology by coupling aeromagnetic with DEM data. We suggest two hierarchical orders of linkage patterns in ORZ: (1) first-order linkage where two or more major sub parallel rift faults are linked by connecting faults (Figures 6 and 7), and (2) second-order linkage that is achieved through soft to hard linkage of small en échelon segments along the axis of a single fault (Figures 4 and 5). For example, segments within portions of the Thamalakane Fault and the Linyanti Fault systems exhibit patterns consistent with the development of soft linkages (Figures 4 and 5). The Chobe Fault shows evidence of a hard linkage forming between two en échelon right-stepping segments leading to abandonment of a portion of the former fault tip (Figure 5). The Kunyere, and Mababe Faults exhibit more continuous faults traces (i.e., fewer segments) indicating a more advanced stage of linkage (Figures 4, 5, 6, and 7). The larger throws on the basement for the Kunyere and Mababe faults (Table 1) are consistent with an advanced stage of fault evolution.

5.3. Development of Border Faults

[28] Border, master or basin faults are defined as faults that bound the rift basins [*Peacock and Sanderson*, 1991, and references therein]. The characteristics of border faults include larger displacement and length when compared to other faults within the same rift. A particular rift zone can have one or multiple border faults depending on the number

of basins within the rift. For example, the Rio Grande Rift has 4 border faults one for each of the four basins that make up the rift, Malawi Rift has four border faults for its four basins [*Ebinger et al.*, 1984; *Chapin and Cather*, 1994]. Following the same definition *Kinabo et al.* [2007] reported that the border fault in the ORZ is still in a juvenile stage. This interpretation was based solely on the vertical displacements along faults obtained from 3-D Euler deconvolution solutions and length of the faults observed on the aeromagnetic data.

[29] Within the ORZ, border faults are still developing through the formation of soft and subsequently hard linkage of several rift-related faults. In addition to linkage of segments along the axes within individual fault zones, linkages are also developing between the major rift faults. The Kunyere Fault is transferring strain to the Thamalakane Fault along a soft linkage defined by a lateral ramp between overlapping segments of these two fault zones (Figure 4) and to the south along a soft linkage characterized by hooking of the fault tips and diffusion of the strain along closely spaced parallel fault segments and a diffuse set of -east-west fractures oriented approximately 75° clockwise from the strike of the main fault zones (Figure 7). The patterns for subsidiary faults and fractures to the main fault traces are consistent with those of Riedel shears associated with right-lateral strike-slip (Figure 10). Thus, the transfer of strain from one fault to other may be influenced by preexisting fractures in the basement as well as a component of right-lateral strike-slip, which for a system of right-stepping faults would lead to extension. It is important to note that the Meso- to Neo-proterozic northwest Botswana Rift has also been suggested to represent a pull-apart basin that formed as a result of dextral shearing [*Aldiss and Carney*, 1992]. Thus, the extent to which the pattern of subsidiary faults and fractures reflects a present-day stress regime with a component of dextral shearing or has inherited this pattern from the basement structures remains unresolved. To the north the Thamalakane Fault partially overlaps the Mababe Fault creating what was initially a soft linkage by transferring strain over a diffuse domain characterized by abundant minor faults and fractures. This soft linkage evolved to a hard linkage as connecting faults between the Thamalakane and Mababe Faults, visible on both the DEM and aeromagnetic map, were established (Figure 6). Here the two faults are left-stepping, which would create a local zone of compression within the area of overlap between the faults if there is indeed a component of right-lateral strike-slip to the displacement. This may explain why the intervening zone is intensely deformed by brittle faults and fractures (Figure 6c). It should be noted that lateral offset of linear markers (e.g., Karroo Dikes) along the fault traces suggest both left lateral and right lateral separation along rift related faults. Additionally, the overall form of the main faults bordering the major deposition centers is left stepping. Thus the extent to which a strike-slip component is significant in the development of the ORZ remains unclear.

[30] Previously, the Kunyere Fault system has been considered the border fault for the ORZ [*Modisi et al.*, 2000]. This interpretation was based on the substantial, nearly continuous length of the fault trace and the significant amount of throw observed on the basement surface (Table 1). However, our analysis of fault linkages suggests that a new master border fault system is emerging through a process of "fault piracy" (the capture of strain from segments of a once prominent older active fault within the interior of the rift by a younger fault along the margin of the rift) defines the new margins of a widening rift. In the ORZ this new master border fault is being created as a result of linkages between portions of the Kunyere Fault system and the Thamalakane Fault system in the south, and the Thamalakane Fault and Phuti Fault systems to the Mababe Fault system along strike to the north. This interpretation is supported by the subdued topographic scarp above the Kunyere Fault which suggests waning displacement along this fault trace (Figure 4). In contrast to the subdued scarp height along the Kunyere, significant topographic fault scarps are present along the Thamalakane and Mababe Faults consistent with recent activity and displacement along these faults. The linking of these large fault systems into a master border fault serves to increase the overall length of the rift by connecting the different depocenters (Figure 3). The older and significantly less active faults (e.g., the Tsau and Lecha faults, Figure 3) occur toward the center of the rift, whereas the younger and more active faults now occur on the margins of the rift (e.g., Thamalakane and Mababe faults, Figure 3). We suggest that the faults located toward the interior of the rift now reside within the strain shadows [see *Cowie*, 1998a] of the larger fault systems developing more toward the exterior of the rift. Thus, the rift also appears to be widening as well as lengthening as it matures by retiring older border faults through fault piracy, (e.g., portions of the Kunyere Fault), through creation of now much larger faults systems (in length) along the new margins of the rift.

[31] *Ringrose et al.* [2005] suggested that 41 ka age represents the best estimate for initiation of active rifting within the ORZ based upon large-scale changes in the drainage pattern of the Okavango River due to vertical movements along rift-related faults. However, the advanced stage of development of fault systems as indicated by their lengths (10s to 100s of kms), as a result of numerous linkages between fault segments, and the emergence of nascent border faults within the ORZ would seem to imply a much older age for initiation of continental rifting in this region. For example, *Cowie* [1998b] used a numerical model to examine nucleation and growth of faults within a homogeneous brittle-elastic medium. The results of this model showed a marked transition from diffuse strain distributed over numerous spatially randomly small (<20 km) fault segments to one of focused strain along a single long (>70 km) fault system that emerged from linking of many small fault segments at ~90 ka of rifting [*Cowie*, 1998b]. While this study demonstrated the importance of the location of faults with respect to neighboring faults in optimizing fault growth, it did not consider the role of preexisting strength anisotropies in the crust on fault growth. The spatial correspondence between the prominent

basement fabric (foliations and fractures) and the orientation of normal faults and linkages suggest that these planar strength anisotropies were in the optimal orientation with respect to the regional stress field to be easily reactivated. The lower critical stress required for brittle failure along these planes would allow faults to propagate further and with greater frequency in comparison to intact rock. This would in turn accelerate the process of creating fault linkages between fault segments to form longer fault systems and at the same time inhibiting the nucleation and development of faults that reside with the strain shadows of the larger faults as described by the model of *Cowie* [1998b]. Thus we suggest the apparent discrepancy in fault lengths and the young age of the ORZ serves to highlight the importance of considering the effect of preexisting strength anisotropies within the crust on fault nucleation, propagation, and growth as well as on the scaling relationships between D_{max} and Length.

5.4. Neotectonics and Fluvial Systems

[32] The main fault zones, the linkages between these zones, and preexisting basement fabrics appear to be exerting a profound influence on the drainage patterns of the fluvial systems in the ORZ. Linkages between major fault zones are commonly areas of intense fracturing that have been influenced by the orientation of basement fabrics and are exploited by stream/river erosion. For example, in the south the Thamalakane River flows along the Thamalakane Fault and exhibits abrupt deflections (rather than smooth meanders) in the orientation of its course (as seen on DEM) that define a pattern of right stepping en échelon river channel segments (Figure 7). South of 20°15′S the river flows in an almost east-west direction, cutting through the Kunyere Fault and into Lake Ngami along NE trending right stepping en échelon segments. In the north, the interaction of the Thamalakane Fault and the Mababe Fault coincides with a NNE trending stream (channel A; Figures 6a and 6b) while the interaction between the Phuti Fault and the Mababe Fault is highlighted by a NNW trending stream channel B (Figures 6a and 6b). Fractures orientation on DEM and aeromagnetic maps display pronounced ~ESE-WNW and also SSW-NNE and SSE-NNW trends coinciding with the trends of the stream channels (Figures 6, 7, and 10). Similarly, a study by *Wormald et al.* [2003] found out that pans are also aligned 030°–050° and 130°. The pans develop along the southern side of the ORZ reflecting the general SE tilt of the faults blocks along listric normal faults (Figure 3 and 10). Hence, it appears that faults and fractures are exerting a profound influence on the location and development of the river/stream channels and pans highlighting the coupling of neotectonic and fluvial activities in the ORZ.

6. Conclusions

[33] The integration of high-resolution aeromagnetic data with DEM data made possible important insights into fault growth and propagation associated with the ORZ. Coupled analysis of SRTM DEM and aeromagnetic data has revealed that (1) the growth of individual rift faults occurs by along axis linkage of small segments; (2) on the basis of the relationship between fault throws and scarp heights, the faults in the ORZ can be categorized into four groups (group a) old and active such as the Thamalakane and Mababe faults, (group b) young and active, for example the Gumare Fault, (group c) faults with no recent activity such as the Lecha and Tsau faults, and (group d) faults with waning activity, for example the Kunyere Fault; (3) young and more active rift faults are located on the outer margin of the rift, whereas old and non active faults are in the middle suggesting that the rift grows both in length (by along axis linkage of segments) and width; (4) a border fault system is developing by linkage of major subparallel rift faults and retirement of portions of other fault segments through fault piracy. This process results in both lengthening and widening of the rift basin; (5) anisotropies present in the basement (basement fractures, faults, foliations) greatly influenced the development of faults associated with the formation of the ORZ, including fault orientations, linkages between fault segments, and extending fault lengths. Utilization of these preexisting zones of weakness allowed faults that are 3–25 km long to link and grow to form major rift faults ~25–325 km long at a very early stage of continental rifting and also explains the apparent paradox between the faults length (25–325 km) versus throw (17–334 m) for this young rift; and (6) coupling of DEM with aeromagnetic data analysis is a powerful tool for studying rift kinematic processes and can significantly augment field studies, especially in areas with limited basement exposures.

[34] **Acknowledgments.** Partial funding for this project was provided by the National Science Foundation (NSF-OISE-0217831 and NSF-OISE-0644836) and the American Chemical Society, Petroleum Research Fund (ACS PRF 38595-AC8). The Geological Survey of Botswana provided magnetic data. Dianwei Ren and Marianne Medina assisted with the remote sensing data processing. Damien Delvaux, Hendratta Ali, Caroline Davis, and Moidaki Moikwathai reviewed an earlier version of the manuscript. Reviews comments of Nancy Dawers and an anonymous reviewer critically improved this paper. This paper is Missouri University of Science and Technology Geology and Geophysics contribution 8.

References

Aldiss, D. T., and J. N. Carney (1992), The geology and regional correlation of the Proterozoic Okwa Inlier, western Botswana, *Precambrian Res.*, *56*, 255–274, doi:10.1016/0301-9268(92)90104-V.

Anders, M. H., and R. W. Schlische (1994), Overlapping faults, intrabasin highs and growth of normal faults, *J. Geol.*, *102*, 165–180.

Briggs, I. C. (1974), Machine contouring using minimum curvature, *Geophysics*, *39*, 39–48, doi:10.1190/1.1440410.

Cartwright, J. A., B. D. Trudgill, and C. S. Mansfield (1995), Fault growth by segment linkage: An explanation for scatter in maximum displacement and trace length data from Canyonlands Graben of SE Utah, *J. Struct. Geol.*, *17*, 1319–1326, doi:10.1016/0191-8141(95)00033-A.

Chapin, C. E., and S. M. Cather (1994), Tectonic setting of the axial basins of the northern and central Rio Grande rift, in *Basins of the Rio Grande Rift: Structure, Stratigraphy, and Tectonic Setting*, edited by G. R. Keller and S. M. Cather, *Spec. Pap. Geol. Soc. Am.*, *291*, 5–25.

Chen, L., and L. Lee (1992), Progressive generation of control frameworks for image registration, *Photogramm. Eng. Remote Sens.*, *58*, 1321–1328.

Cowie, P. A. (1998a), Normal fault growth in three dimensions in continental and oceanic crust, *Geophys. Monogr.*, *106*, 325–345.

Cowie, P. A. (1998b), A healing-reloading feedback control on the growth rate of seismogenic faults, *J. Struct. Geol.*, *20*, 1075–1087, doi:10.1016/S0191-8141(98)00034-0.

Cowie, P. A., and C. H. Scholz (1992), Displacement-length scaling relationships for faults: Data synthesis and discussion, *J. Struct. Geol.*, *14*, 1149–1156, doi:10.1016/0191-8141(92)90066-6.

Davies, S. J., N. H. Dawers, A. E. McLeod, and J. R. Underhill (2000), The structural and sedimentological evolution of early synrift succession: The Middle Jurassic Tarbert Formation, North Sea, *Basin Res.*, *12*, 343–365, doi:10.1046/j.1365-2117.2000.00136.x.

Dawers, N. H., and M. H. Anders (1995), Displacement-length scaling and fault linkage, *J. Struct. Geol.*, *17*, 607–614, doi:10.1016/0191-8141(94)00091-D.

Dawers, N. H., M. H. Anders, and C. H. Scholz (1993), Growth of normal faults: Displacement-length scaling, *Geology*, *21*, 1107–1110, doi:10.1130/0091-7613(1993)021<1107:GONFDL>2.3.CO;2.

Ebinger, C. J., M. J. Crow, B. R. Rosendahl, D. A. Livingstone, and J. LeFournier (1984), Structural evolution of Lake Malawi, *Nature*, *308*, 627–629, doi:10.1038/308627a0.

Ebinger, C., Y. Poudjom Djomani, E. Mbede, A. Foster, and J. B. Dawson (1997), Rifting Archaen lithosphere: The Eyasi-Natron rifts, East Africa, *J. Geol. Soc.*, *154*, 947–960, doi:10.1144/gsjgs.154.6.0947.

Fairhead, J. D., and R. W. Girdler (1969), How far does the rift system extend through Africa?, *Nature*, *221*, 1018–1020, doi:10.1038/2211018a0.

Fairhead, J. D., and N. B. Henderson (1977), The seismicity of southern Africa and incipient rifting, *Tectonophysics*, *41*, 19–26, doi:10.1016/0040-1951(77)90133-0.

Foster, A., C. Ebinger, E. Mbede, and D. Rex (1997), Tectonic development of the northern Tanzanian sector of the East African Rift System, *J. Geol. Soc.*, *154*, 689–700, doi:10.1144/gsjgs.154.4.0689.

Gawthorpe, R. L., I. Sharp, J. R. Underhill, and S. Gupta (1997), Linked sequence stratigraphic and structural evolution of propagating normal faults, *Geology*, *25*, 795–798, doi:10.1130/0091-7613(1997)025<0795:LSSASE>2.3.CO;2.

Grauch, V. J. S. (2001), High-resolution aeromagnetic data, a new tool for mapping intrabasinal faults: Example from the Albuquerque basin, New Mexico, *Geology*, *29*, 367–370, doi:10.1130/0091-7613(2001)029<0367:HRADAN>2.0.CO;2.

Jackson, C. A., R. B. Gawthorpe, and I. R. Sharp (2002), Growth and linkage of the East Tanka fault zone, Suez Rift: structural style and synrift stratigraphic response, *J. Geol. Soc.*, *159*, 175–187.

Kampunzu, A. B., P. Akanyang, R. B. M. Mapeo, B. N. Modie, and M. Wendorff (1998), Geochemistry and tectonic significance of the Mesoproterozoic Kgwebe metavolcanic rocks in northwest Botswana: Implications for the evolution of the Kibaran Namaqua-Natal Belt, *Geol. Mag.*, *135*, 669–683, doi:10.1017/S001675689800123X.

Kervyn, F., S. Ayub, R. Kajara, E. Kanza, and B. Temu (2006), Evidence of recent faulting in the Rukwa rift (West Tanzania) based on radar interferometric DEM, *J. Afr. Earth Sci.*, *44*, 151–169, doi:10.1016/j.jafrearsci.2005.10.008.

Key, R. M., and N. Ayres (2000), The 1998 edition of the national geological map of Botswana, *J. Afr. Earth Sci.*, *30*, 427–452, doi:10.1016/S0899-5362(00)00030-0.

Kinabo, B. D., E. A. Atekwana, J. P. Hogan, M. P. Modisi, D. D. Wheaton, and A. B. Kampunzu (2007), Early structural evolution of the Okavango Rift Zone, NW Botswana, *J. Afr. Earth Sci.*, *48*, 125–136, doi:10.1016/j.jafrearsci.2007.02.005.

Le Calvez, J. H., and B. C. Vendeville (2002), Physical modeling of normal faults and grabens above relay above salt, *Trans. Gulf Coast Assoc. Geol. Soc.*, *52*, 599–606.

Le Gall, B., G. Tshoso, F. Jourdan, G. Fèraud, H. Bertrand, J. J. Tiercelin, A. B. Kampunzu, M. P. Modisi, J. Dyment, and M. Maia (2002), $^{40}Ar/^{39}$ geochronology data from the giant Okavango and related mafic dyke swarms, Karoo igneous province, northern Botswana, *Earth Planet. Sci. Lett.*, *202*, 595–606, doi:10.1016/S0012-821X(02)00763-X.

Macheyeki, A. S., D. Delvaux, F. Kervyn, and E. B. Temu, (2005), Morphotectonics of the Kanda Fault System in the Ufipa Plateau between Tanganyika and Rukwa Rift Basins, SW-Tanzania, in *Extended Abstracts on the International Conference on the East African Rift System*, edited by E. Atekwana et al., pp. 53–57, Univ. of Dar es Salaam, Mbeya, Tanzania.

McClay, K. R., T. Dooley, P. Whitehouse, and M. Mills (2002), 4-D evolution of rift systems: Insights from scaled physical models, *Am. Assoc. Pet. Geol. Bull.*, *86*(6), 935–959.

Modie, B. N. (2000), Geology and mineralization in the Meso- to Neoproterozoic Ghanzi-Chobe Belt of northwest Botswana, *J. Afr. Earth Sci.*, *30*, 467–474, doi:10.1016/S0899-5362(00)00032-4.

Modisi, M. P., E. A. Atekwana, A. B. Kampunzu, and T. H. Ngwisanyi (2000), Rift kinematics during the incipient stages of continental extension: Evidence from the nascent Okavango rift basin, northwest Botswana, *Geology*, *28*, 939–942, doi:10.1130/0091-7613(2000)28<939:RKDTIS>2.0.CO;2.

Morley, C. K. (1999), How successful are analogue models in addressing the influence of pre-existing fabrics on rift structure?, *J. Struct. Geol.*, *21*, 1267–1274, doi:10.1016/S0191-8141(99)00075-9.

Morley, C. K. (2002), Evolution of large normal faults: Evidence from seismic reflection data, *Am. Assoc. Pet. Geol. Bull.*, *86*(6), 961–978.

Moustafa, A. R. (2002), Controls on the geometry of transfer zones in Suez rift and northwest Red Sea: Implication for the structural geometry of rift systems, *Am. Assoc. Pet. Geol. Bull.*, *86*(6), 979–1002.

Mulugeta, G., and G. Woldai (2001), Modeling heterogeneous stretching during episodic or steady rifting of the continental lithosphere, *Geology*, *29*, 895–898, doi:10.1130/0091-7613(2001)029<0895:MHSDEO>2.0.CO;2.

Nash, D. B. (1986), Morphological dating and modeling degradation of fault scarps, in *Active Tectonics: Impact on Society*, pp. 181–194, Natl. Academy Press, Washington, D. C.

Peacock, D. C. P., and D. J. Sanderson (1991), Displacements, segment linkage and relay ramps in fault zones, *J. Struct. Geol.*, *13*, 721–733, doi:10.1016/0191-8141(91)90033-F.

Ring, U. (1994), The influence of preexisting structure on the evolution of the Cenozoic Malawi rift (East African Rift System), *Tectonics*, *13*, 313–326, doi:10.1029/93TC03188.

Ringrose, S., P. Huntsman-Mapila, A. B. Kampunzu, W. Downey, S. Coetzee, B. Vink, W. Matheson, and C. Vanderpost (2005), Sedimentological and geochemical evidence for paleo-environmental change in the Makgadikgadi subbasin, in relation to the MOZ rift depression, Botswana, *Paleogeogr. Palaeoclimatol. Palaeoecol.*, *217*, 265–287, doi:10.1016/j.palaeo.2004.11.024.

Schlische, R. W., and M. H. Anders (1996), Stratigraphic effects and tectonic implications of the growth of normal faults and extensional basins, in *Reconstructing the Structural History of Basin and Range Extension Using Sedimentology and Stratigraphy*, edited by K. K. Beratan, *Spec. Pap. Geol. Soc. Am.*, 303, 183–203.

Schlüter, T. (2006), *Geological Atlas of Africa, With Notes on Stratigraphy, Tectonics, Economic Geology, Geohazards, and Geosites of Each Country*, 272 pp., Springer, New York.

Scholz, C. H., T. A. Koczynski, and D. G. Hutchins (1976), Evidence for incipient rifting in southern Africa, *Geophys. J. R. Astron. Soc.*, *44*, 135–144.

Schwartz, M. O., Y. Y. Kwok, D. W. Davis, and P. Akanyang (1996), Geology, geochronology and regional correlation of the Ghanzi Ridge, Botswana, *South Afr. J. Geol.*, *99*, 245–250.

Swain, C. J. (1976), A FOTRAN IV program for interpolating irregularly spaced data using the difference equations for minimum curvature, *Comput. Geosci.*, *1*, 231–240, doi:10.1016/0098-3004(76)90071-6.

Trudgill, B. D., and J. A. Cartwright (1994), Relay ramp forms and normal fault linkage Canyonlands National Park, Utah, *Geol. Soc. Am. Bull.*, *106*, 1143–1157, doi:10.1130/0016-7606(1994)106<1143:RRFANF>2.3.CO;2.

Trudgill, B., and J. R. Underhill (2002), Introduction to the structure and stratigraphy of rift systems, *Am. Assoc. Pet. Geol. Bull.*, *86*(6), 931–933.

Walsh, J. J., W. R. Bailey, C. Childs, A. Nicol, and C. G. Bronson (2003), Formation of segmented normal faults: A 3-D perspective, *J. Struct. Geol.*, *25*, 1251–1262, doi:10.1016/S0191-8141(02)00161-X.

Withjack, M. O., Q. T. Islam, and P. R. La Pointe (1995), Normal faults and their hanging-wall deformation: An experimental study, *Am. Assoc. Pet. Geol. Bull.*, *79*(1), 1–18.

Wormald, R. J., F. D. Eckardt, J. Vearncombe, and S. Vearncombe (2003), Spatial distribution of pans in Botswana: The importance of structural control, *S. Afr. J. Geol.*, *106*, 287–290, doi:10.2113/106.4.287.

M. G. Abdelsalam and J. P. Hogan, Department of Geological Sciences and Engineering, Missouri University of Science and Technology, 129 McNutt Hall, Rolla, MO 65409, USA.

E. A. Atekwana, Oklahoma State University, Boone Pickens School of Geology, 105 Noble Research Center, Stillwater, OK 74078, USA. (estella.atekwana@okstate.edu)

M. P. Modisi, Department of Geology, University of Botswana, Private Bag 0022, Gaborone, Botswana.

B. D. Kinabo, Technical Geophysics Group, Deepwater Gulf of Mexico, Chevron North America Exploration and Production, 1500 Louisiana St., Houston, TX 77002, USA.